Research article

Effects of interfacial interactions between metal and process control agents during ball milling on the microstructure of the milled Fe-based nanocrystalline alloy powder

Satoshi Motozuka [a,*], Hisashi Sato [b], Hidenori Kuwata [c], Mitsuo Bito [c], Yasuo Okazaki [d]

[a] Department of Science and Engineering, Kyushu Institute of Technology, 1-1 sensui-cho, Tobata-ku, Kitakyushu, 804-8550, Japan
[b] Graduate School of Engineering, Nagoya Institute of Technology, Gokiso-cho, Showa-ku, Nagoya, 466-8555, Japan
[c] Tohoku Magnet Institute, Katahira, Aoba-ku, Sendai, 980-0812, Japan
[d] Department of Materials and Science and Technology, Gifu University, Yanagido, Gifu, 501-1193, Japan

ARTICLE INFO

ABSTRACT

Fe–Si–B–P–Cu nanocrystalline alloy were treated with ball-mill using a lubricant as a process control agent (PCA). The resulting alloy powder is a strong candidate material for soft magnetic composites. Two ball milling methods (continuous and interval) were employed to control the interactions between the PCA and the alloy surface, and their effect on the microstructure of the prepared alloy particles was investigated. The alloy sheet was broken into small pieces and deformed plastically into flake-shaped particles regardless of the ball milling method implemented. Friction-force microscopy of the alloy immersed in the PCA revealed that the friction coefficient of the alloy surface exposed to air for a certain period was higher than that of the unexposed alloy surface (immediately after polishing). During ball milling, the ratio of the newly generated surface to the oxidized surfaces of the alloy subjected to interval milling was smaller than that of the alloy subjected to continuous milling. Therefore, the friction coefficient of the surface of the alloy subjected to interval milling was higher than that of the alloy subjected to continuous milling. Synchrotron radiation analysis revealed that the alloy subjected to interval milling exhibited enhanced surface friction, showing an obvious steepness and inflection in the diffraction intensity as a function of the tilt angle based on the Schulz reflection method. This indicates formation of crystallographic texture in α-Fe grains in an amorphous matrix. Hence, we demonstrated successfully that the ball milling process induced a crystallographic texture in the Fe-based nanocrystalline alloy due to plastic deformation due to the enhanced surface friction. The surface of the alloy was prepared based on the effect of the interfacial interactions between the alloy surface and the PCA.

1. Introduction

Fe–Si–B–P–Cu nanocrystalline alloy exhibit excellent soft magnetic properties; thus, their sheets are ideal candidates for iron cores to improve the efficiency of electric motors (Makino et al., 2011). Such Fe cores are fabricated by laminating the sheets of the desired materials. A large amount of scrap is generated during the fabrication of Fe cores. Soft magnetic composites (SMCs) are artificial aggregates of ferromagnetic powders. Powders obtained from ball milled alloy scrap are potential SMCs. Flake shaped powders have better magnetic properties owing to the suppressed demagnetizing field due to magnetic shape anisotropy (David, 1998). However, nanocrystalline alloys are brittle; thus, powders obtained from ball milling have random geometry.

To obtain flake powders from nanocrystalline alloy sheets through ball milling, the sheets must be crushed and plastically deformed. Even in brittle materials (e.g., metallic glass and intermetallic), particles can be deformed plastically into platelet shape by ball-mill treatment using a process control agent (PCA), such as an organic solvent or oil, which controls the surface energy on the particles (Koch and Whittenberger, 1996; Niu, 2020). The effects of ball milling on the structure and magnetic properties of soft ferromagnetic metallic glasses have been widely studied (He et al., 1995; Bednarcik et al., 2004; Ramasamy et al., 2017). However, only a few studies have investigated the effects of PCA on the deformation behavior of Fe-based nanocrystalline alloys during ball milling.

---

* Corresponding author.
E-mail address: motozuka@post.matsc.kyutech.ac.jp (S. Motozuka).

For electromagnetic steel sheet applications, the magnetic properties of the sheets can be improved by controlling the crystallographic texture in the (001) plane parallel to the surface of the sheets by maximizing the area of (100) planes in the easy magnetization axes (David, 1998; Tomida, 1996). Annealing under a magnetic field can convert the microstructure of the sheets to the preferred crystallographic orientation called texture. Fujii et al. (2006) reported the evolution of a sharp {110} texture in Fe-based nanocrystalline alloys during recrystallization from the amorphous phase under a magnetic field of 6 T and a temperature of 853 K. However, the process that can induce the texture on nanocrystalline alloys has not been reported yet.

For conventional coarse-grained polycrystalline Fe powders, flakes and textures in the (001) planes of α-Fe oriented parallel to the flake shape have been formed through ball milling using a lubricant as the PCA. The texture obtained by ball milling was deformation texture through uniaxial compression or multidirectional-rolling-like deformation (Motozuka et al., 2015). Lubricants reduce the shear force on the particle surfaces by suppressing the formation of other textures derived from the shear force localized on the surfaces, forming Fe particles with a uniform texture (Motozuka et al., 2017).

The deformation texture forms generally by dislocation glide through grains (Humphreys and Hatherly, 2012). Therefore, in the case of brittle materials, which deform plastically through grain boundary–mediated processes without dislocation glides through grains, deformation textures are not formed (Ovid'ko and Sheinerman, 2008). Cui et al. (2011) processed the brittle SmCo₅ powder through high-energy ball milling using heptane (as the PCA) with oleic acid. They deformed the material into flakes with a texture in the (200) planes oriented parallel to the flakes and showed that the addition of the oleic acid to the heptane (PCA) promoted texture formation. However, the detailed mechanism of texture formation was not revealed.

Oleic acid improves the oiliness by adsorbing onto substrates and reducing friction (Doig et al., 2014). It can be expected that the mechanism of texture formation with surface lubrication is different from that of ductile materials. Herein, to obtain Fe-based nanocrystalline alloy powders with better magnetic properties, an alloy sheet was ball milled in the presence of a PCA and then the interfacial interactions, including the friction between the Fe alloy and PCA, were controlled. Effect of the interaction on the type of deformation as well as the resulting microstructures obtained through ball milling were investigated.

2. Materials and methods

Fe–Si–B–P–Cu (NANOMET®) nanocrystalline alloy sheet was used herein (Makino et al., 2011). The melt-spun Fe–Si–B–P–Cu alloy was partially crystallized by heat treatment for embrittlement. Petroleum ether (fraction 60°C–70 °C) and acetone (>99.0% purity; Nacalai Tesque Inc.) were used as received.

The NANOMET® sheet was crushed into 5-mm-sized pieces. Subsequently, 6.3 g of the pieces, 375 g of steel balls (AISI 52100; diameter = 4 mm) were put into a stainless steel vessel for ball-milling appratus. As a PCA, 20 mL of oil (5–56 from KURE Engineering Co. with the main contents of antirust oil [CAS registry No. 64741-88-4], hydrocarbon solvent [CAS No.64742–47-8], propane [CAS No. 74-08-6], and isobutane [CAS No. 75-28-5]) were also added. Milling treatments were carried out using an attrition mill Powder Laboratory (Nippon Coke and Engineering Co.), which was operated at 1000 rpm. With the PCA, the friction coefficient of the newly generated alloy surfaces, which were formed by both polishing and plastic deformation, was lower than that of the alloy surfaces exposed to the atmosphere for a certain period. Due to the characteristic microtribological behavior of the alloy surfaces, the alloy pieces were ball milled continuously for 30 min. Hereafter, the milling process is referred to as "continuous milling." The newly generated alloy surfaces were formed continuously during the process; therefore, continuous milling maintained a low friction coefficient on the alloy surfaces during ball

milling. For comparison, the alloy pieces were ball milled for 6 min and subsequently washed sequentially in 30 ml of petroleum ether and acetone. Thereafter, the milled sample was exposed to the atmosphere for one week. The procedure was repeated five times with a cumulative milling time of 30 min. Hereafter, the intermittent milling method is referred to as "interval milling." The newly generated alloy surface formed during ball milling was exposed to the atmosphere, and the friction coefficient of the exposed surface was high; thus, the interval milling maintained a high friction coefficient on the alloy surface during the process.

The microtribological features on the alloy surface were evaluated using a scanning probe microscope (SPM; AFM5100N, Hitachi High-technologies Co.) in the lateral modulation friction-force microscope (LM-FFM) mode. An SI-DF3-P2 probe (Hitachi High-technologies Co) was used in the LM-FFM analysis. The frequency and the modulation amplitude of the probe during a scan were 5 kHz and 10 nm, respectively. A detailed description of the LM-FFM mode can be found in previous reports (Iizuka et al., 2004; Mizuno and Ando, 2010; Miyake et al., 2006). Briefly, samples of the alloy sheets were polished mechanically using emery papers and diamond paste and subsequently washed in acetone. The polished alloy sheets were immersed in the PCA, after which the surfaces were scanned using a probe. Immediately after scanning, the alloy sheets were washed sequentially in petroleum ether and acetone to remove the PCA on the surfaces and subsequently exposed to the atmosphere for certain period of time. Next, the microtribological behavior of the exposed alloy sheet surfaces was evaluated again. Since the surfaces of the alloy particles obtained through interval milling were prepared similarly, the measured microtribological behavior of the exposed surfaces represents the surface of the alloy particles obtained using interval milling.

The alloy sheets were observed using scanning electron microscopy (SEM, ERA-8800, Erionix Inc.) and scanning transmission electron microscopy (STEM, ARM200F, JEOL Ltd.). The true strain (ε_t) was estimated using Eq. (1).

$$\varepsilon_t = \ln \frac{l}{l_0}, \tag{1}$$

where l_0 and l are the thicknesses of the sample before and after milling, respectively. The thicknesses were estimated by the SEM images. The ball milled alloy sheet deformed plastically to flake-shaped particles (Motozuka et al., 2021). The average particle size was defined as the diameter of a circle circumscribed by flake-shaped particles. The flakes have a disk shape. The specific surface area of the particles was estimated from the average particle size and thickness of the disk. The thickness of the alloy sheet before ball milling was about 25 μm. The area of the disk was estimated as the area of the upper and bottom sides of a cylinder with the same height as the alloy sheet and the same volume as the flake particles. The area of the newly generated alloy surface obtained by ball milling was estimated from the difference in the area of the upper and lower surfaces of the cylinder from the surface area of the disk.

Synchrotron X-ray diffraction (XRD) were performed using beam line BL8S1 at the Aichi Synchrotron Radiation Center. The isotropic strains in the samples were estimated using the following Williamson–Hall equation (Williamson and Hall, 1953):

$$\beta\cos\theta = \frac{K\lambda}{D} + 4\varepsilon\sin\theta, \tag{2}$$

where β, K, λ, D, θ, and ε are the full-width-at-half-maximum of a diffraction peak, the shape factor (0.9), X-ray wavelength (0.96 Å), crystallite size, Bragg's angle, and microstrain respectively. Therefore, the strain is determined as the slope of a $\beta\cos\theta$–$\sin\theta$ plot. The XRD patterns revealed an amorphous halo and the Williamson–Hall (WH) plots were generated from the diffraction patterns using integrated X-ray powder diffraction software from Rigaku. The XRD patterns were fitted to the split Pearson VII function (Elderton and Johnson, 1969). The

texture of the milled powder was determined using synchrotron radiation produced via the Schulz reflection method (Schulz, 1949).

3. Results and discussion

Atomic force microscopy (AFM) and LM-FFM (lateral force) images of the samples are shown in Figure 1(a-1 to a-4) and 1(b-1 to b-4), respectively. The nanocrystalline alloy samples without (just after polishing) and with 24-, 48-, and 168-h exposure to the atmosphere are shown in Figures 1(a-1, b-1), 1(a-2, b-2), 1(a-3, b-3), and 1(a-4, b-4), respectively. Cross sections along the white lines on the lateral force images are shown in Figure 1(c). AFM revealed the unevenness of approximately 100 nm on the surface of each sample. No systematic changes in the unevenness were observed with the increasing atmospheric exposure time. On visual inspection, all the samples showed a similar metallic luster. However, the lateral force images obtained for the samples with and without atmospheric exposure were different. Few signals were detected from the surface of the alloys just after polishing. Thus, there were no patterns on the lateral force image (Figure 1(b-1)). The lateral force image for the sample exposed for 24 h shows a pattern along the polishing mark extending from the lower left to the upper right side. The sheets exposed for 48 and 168 h showed a granular pattern having a size of about 30 nm. Changes in the signal intensity along the white line were observed on the lateral force image (Figure 1(c)). The signal intensities obtained from the surfaces of all the alloys exposed for over 24 h were more than two times larger than those of the alloy samples without exposure. Therefore, exposing the alloys to the atmosphere increased the friction coefficient of their surfaces.

Figure 2. TEM image of neat nanocrystalline alloy.

Figure 1. Representative (a-1 to a-4) AFM and (b-1 to b-4) LM-FFM (lateral force) images of the nanocrystalline alloy samples (a-1, b-1) just after polishing, (a-2, b-2) after 24 h, (a-3,b-3) 48 h, and (a-4, b-4) after 168 h. (c) Cross sections of the lateral forces along the line on the images.

Figure 2 shows the bright-field TEM image of the alloy sheet sample before milling. The alloy comprised α-Fe grains in an amorphous matrix. The average grain size (~20 nm) well agreed with the period of the granular pattern in the lateral force images of the milled alloys exposed to the atmosphere [Figure 1(b-3) and (b-4)]. The growth rate of the oxide layer was determined from the crystal plane of the iron surface due to the lattice matching between Fe and oxides (Gulbransen and Ruka, 1952). The formation rates of oxide follow the order (100) > (111) > (110) (Boggs et al., 1967). Based on the effect of lattice mismatch on the oxide growth rate, the oxide growth rate on amorphous and α-Fe grain surfaces may be different. Additionally, the lubricating effects following the interfacial interactions between the lubricant oil and bare metal or oxidized surfaces are different (Buckley, 1981). Therefore, it is considered that the lateral force on the exposed alloy surfaces was higher than that on the unexposed surfaces because of the oxide formed on the surface. The formation rate of oxides affecting the lateral force differs between amorphous and α-Fe grain surfaces; therefore, a pattern with a pitch of several tens of nanometers, which is consistent with the grain size of nanocrystals, appeared in the lateral force images. As ambient air contains not only oxygen but also water, nitrogen, and other components, various iron compounds, such as hydroxides and nitrides could affect the friction coefficient. However, the mechanism behind the increase in the friction coefficient is beyond the scope of this paper. Herein, we focused mainly on the effects of the friction coefficient on the formation of the deformed textures on the nanocrystalline alloy during ball milling. Studies on the aforementioned mechanism are ongoing in our laboratory.

Figure 3 is a set of micrographs showing plane structures (a-1, b-1) and cross-sectional structures (a-2, b-2) of samples before (a-1, a-2) and after (b-1, b-2) milling. Before ball milling, the thickness of the alloy sheets was approximately 25 μm. After ball milling, the alloy sheet pieces were crushed and deformed into flakes. The particles processed by continuous and interval milling showed the same appearance. The measured average sizes of the particles obtained by continuous and interval milling were 35.8 ± 7.5 and 36.1 ± 10.2 μm, respectively, and the thicknesses were 1.8 ± 0.8 and 3.0 ± 1.4 μm, respectively. According to Eq. (1), true strains of the particles were -2.1 and -2.6. The estimated

surface areas showed that 93.5% of the particle surfaces were generated after 30 min of continuous milling. The average size and thickness of the particles obtained throught the fourth interval milling were 27.6 and 4.1 μm, respectively. Estimation of the specific surface area by considering the particle as a disk, revealed that the surface area of the particle after the fifth milling was approximately 20% higher than that after the fourth milling. Therefore, the proportion of the newly generated surface area obtained by interval milling was one-fifth of the area obtained by continuous milling. The standard deviations of the particle size and thickness after the first to the third milling processes were high; therefore, it was difficult to estimate the proportion of the newly generated surface area of the particles. As for the lateral force images in Figure 1, the tribological behavior of the newly generated surface (just after polishing) and the oxidized surface of the alloy were significantly different, and the oxidized surface showed a larger lateral force, indicating a higher friction coefficient in the oxidized surface than the newly generated surface. Therefore, by changing the proportion of the newly generated surface, the tribological behavior of the alloy particle surface during milling can be controlled. We infer that the friction coefficient of the alloy surface obtained by interval milling was higher than that of the surface obtained by continuous milling.

Figure 4(a) displays XRD patterns of the alloy sheet before and after milling. The WH plots derived from the XRD patterns are depicted in Figure 4(b). The detailed curve fitting results of the XRD patterns are shown in Figure 4(c). All Bragg peaks in both patterns were attributed to α-Fe and were superimposed on an amorphous halo belonging to the nanocrystalline phase (Takenaka et al., 2016) in both patterns (Figure 4(a)). No peaks were assigned to the austenite Fe phase, indicating insignificant contamination of the powder samples from the stainless milling vessel. The alloys milled by both methods showed broader full-widths-at-half maxima than the alloy sheet before milling, indicating an increased number of lattice defects in the α-Fe grains. The alloys milled by both methods yielded WH plots with higher slopes and lowere *y*-intercepts than the alloys before milling [Figure 4(b)] suggesting increased microstrain and grain size in the crystalline α-Fe grains, respectively (Williamson and Hall, 1953).
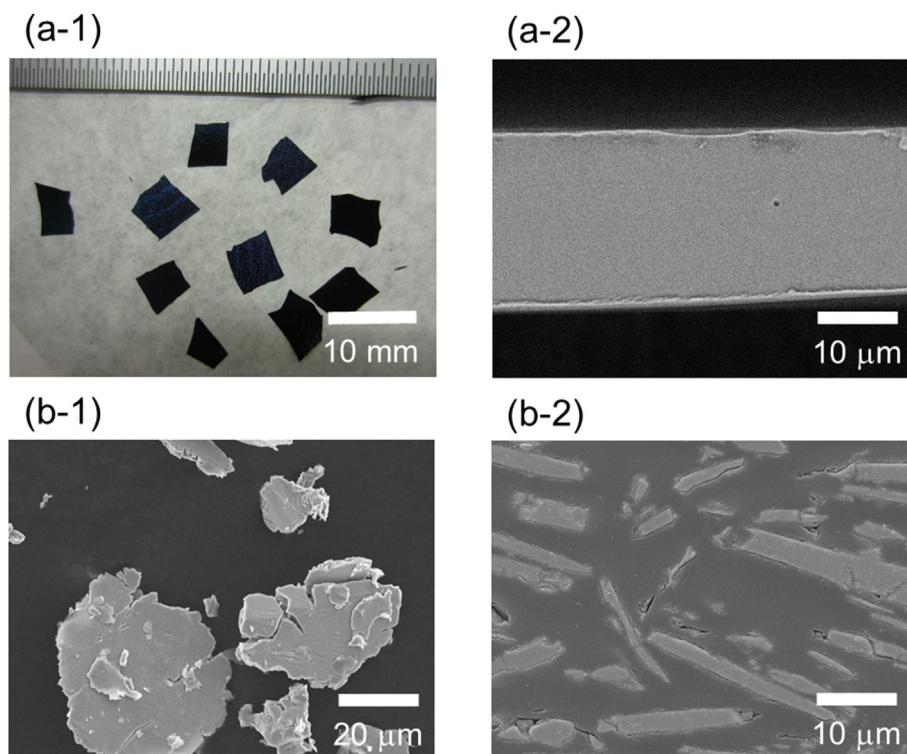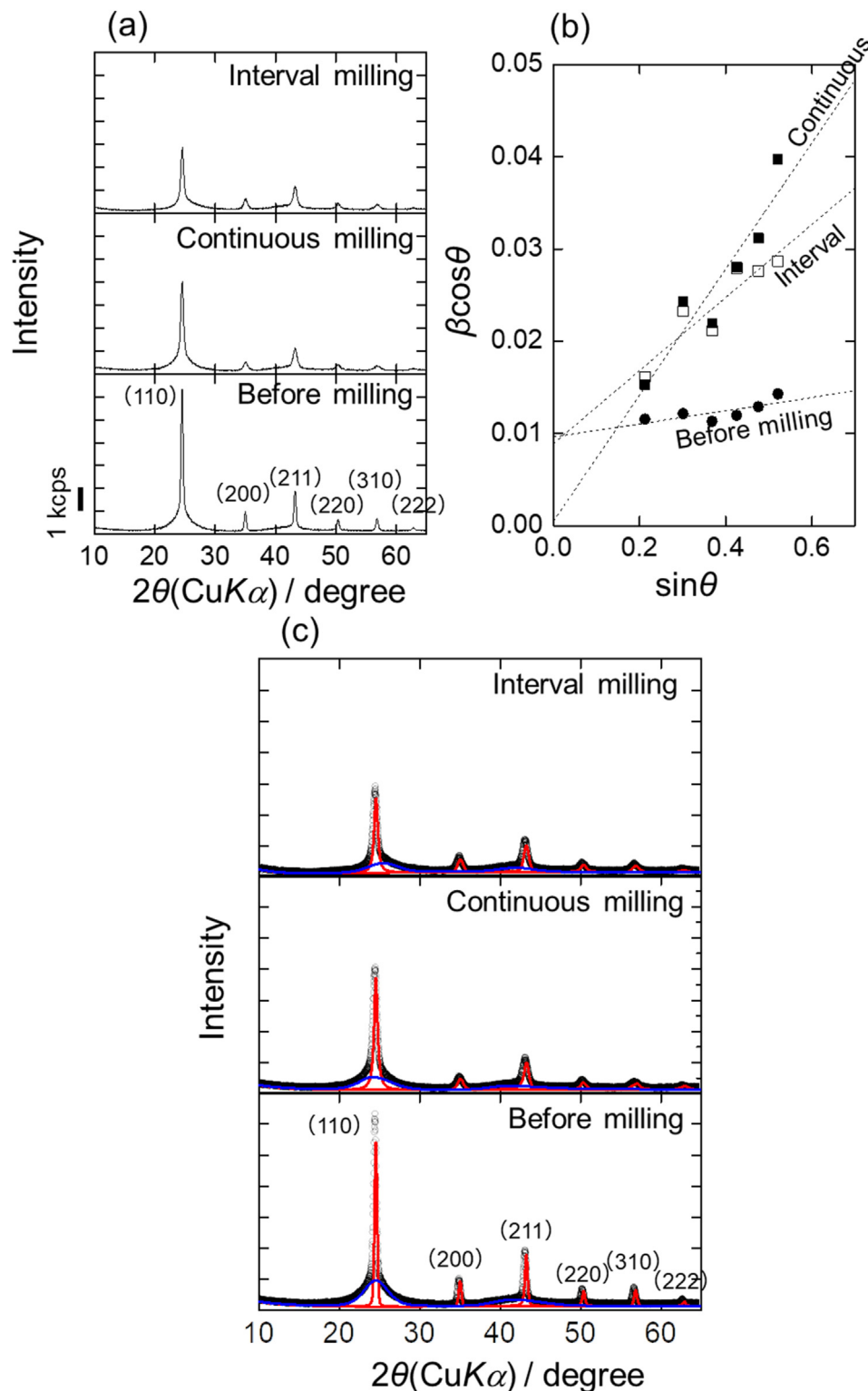

Figure 3. Representative (a-1, b-1) plane structures and (a-2, b-2) cross-sectional structures of the nanocrystalline alloy (a-1, a-2) before and (b-1, b-2) after milling.

Figure 4. (a) Representative X-ray diffraction (XRD) patterns and (b) Williamson–Hall plots derived from the XRD patterns of the nanocrystalline alloy samples before and after milling and (c) detailed curve fitting results of the XRD patterns. Black marks show the measured data, and red lines indicate the fitting curve of α-Fe and amorphous halo.

Figure 5(a-1) and 5(b-1) show the high-angle annular dark-field (HAADF)–STEM images of alloy powders obtained using continuous and interval milling, respectively. Both the milled alloy powder samples contained α-Fe grains in an amorphous matrix. The average sizes and standard deviations of the α-Fe grains in the samples were determined using the TEM images. According to Eq. (2), the grain size of the alloy

before and after continuous and interval milling were 19.1 ± 2.6, 19.5 ± 2.7, and 21.8 ± 3.5 nm, respectively. There is no significant difference in grain size as expected from the Williamson–Hall plots of the samples (Figure 4(b)). The high-magnification images of each sample are shown in Figures 5(a-2) and 5(b-2). and Figures 5(a-3) and (b-3) show high-magnification images of the red frame. Few point, line, and planer
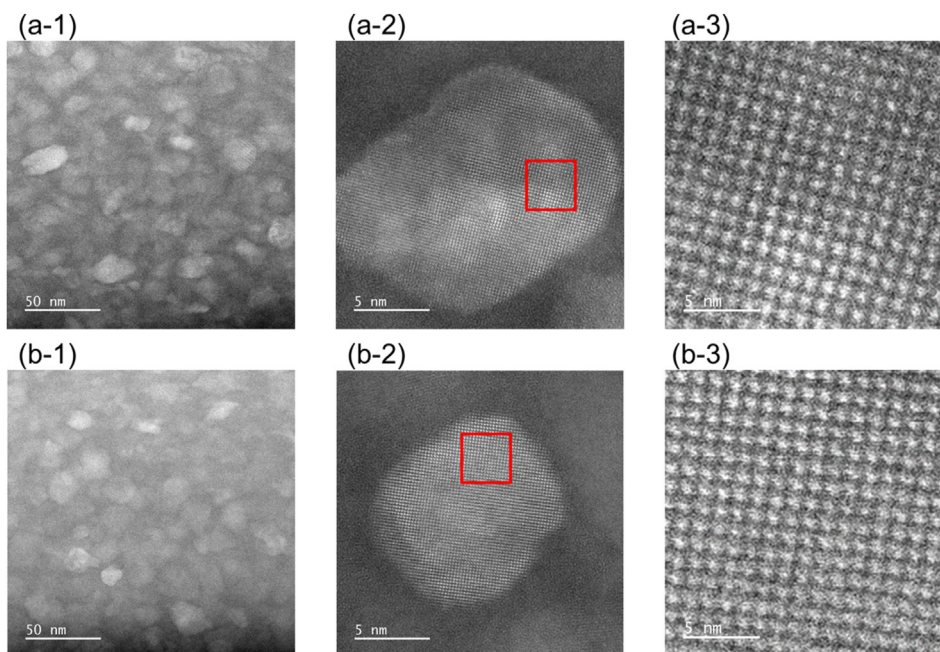
Figure 5. Representative HAADF-STEM images of the alloy samples after (a-1) continuous and (b-1) interval milling. (a-2, a-3, b-2, b-3) are the magnified images of the samples.

defects were observed in the α-Fe grains. The dislocation densities of the alloys were estimated using the modified Williamson–Hall plots (Takaki et al., 2019). The densities for the continuous and interval milled samples were 2.6×10^{17} and 1.2×10^{17} m^{-2}, corresponding to 0.26 and 0.12 nm/nm^3, respectively. However, few lattice defects, such as dislocations, were observed in the grains with a diameter of approximately 20 nm and a volume of approximately 4,000 nm^3, assuming spheres, as shown in Figures 5(a-2) and 5(b-2). The microstrain derived from the slope of the WH plot [Figure 4(b)] likely resulted from lattice distortions due to the elastic strain. Thus, ball milling induced severe plastic deformation and formed a microstructure with a lattice strain and few lattice defects in the alloy.

Owing to the small grain size, dislocations in the grains of nanocrystalline alloys are subjected to strong mutually repulsive forces that are inversely proportional to the distance between the dislocations (Nieh and Wadsworth, 1991). The dominant mechanism in nanocrystalline metals is probably mediated by the grain boundaries, in contrast to dislocation slide in the grains of coarse-grained polycrystalline metals (Schuh et al., 2002). Wang et al. (2014) performed tensile load tests on a nanocrystalline platinum sample under TEM observation. They found that the plasticity mechanism changes from conventional dislocation glide in larger grains (diameter d > 6 nm) to coordinated rotation of multiple grains with d < 6 nm. However, the grain size of the plasticity-mechanism transition has not been experimentally reported in iron or iron-based alloys, although Joon and co-workers estimated a transition grain size of 15 nm based on molecular dynamics simulations (Jeon et al., 2011). Given the small grain size, we thus assumed that few lattice defects existed in the α-Fe grains.

Plastic deformation leads to the evolution of the grain-boundary atomic state and simultaneous relaxation (Hasnaoui et al., 2002). Crystal grains are thought to be surrounded by various boundaries and undergo different relaxations. Crystal grains surrounded by relaxed boundaries are therefore distorted elastically (Gleiter, 1991). We considered that the grain-boundary-relaxation-mediated elastic distortion is related to the slope of the Williamson–Hall plot. A discussion on the deformation mechanism is beyond the scope of this paper, but we are confident that grain-boundary slip is a dominant mechanism that

induced plastic deformation of the alloy during the ball-milling process (Motozuka et al., 2021).

The changes in the relative diffraction intensity of synchrotron radiation of an alloy before milling and after continuous, and interval milling as a function of the tilt angle in the Schulz reflection method are shown in Figure 6. The diffraction intensities of the alloy before and after continuous milling decreased gradually with the decrease in the tilt angle. An irradiated spot of the radiation on the surface of the sample changed as a function of both tilt and Bragg angles. This resulted in a defocusing effect, which is a change in the diffraction intensity irrespective of crystallographic structure of the sample (Kocks et al., 1998). The gradual decrease in the diffraction intensity of the alloy before and after continuous milling was most likely caused by the defocusing effect. Meanwhile, the decrease in the diffraction intensity of the alloy after interval milling was obviously steeper than the others. Furthermore, the diffraction intensity curves of (110) and (200), which were observed in the alloy after interval milling showed inflections at around 45°. These trends were not explained by the defocusing effect and optical geometry. Therefore, the steep diffraction intensity of the alloy that was milled by interval milling was likely caused by a crystallographic orientation.

The Fe-based nanocrystalline alloy was plastically deformed during the ball-milling treatments. Grain-boundary-mediated processes, such as grain-boundary diffusion/sliding/migration and grain rotation, are considered to induce plastic deformation (Motozuka et al., 2021) and likely caused super-plasticity in the plastic deformation of the nanocrystalline alloy. During a superplastic deformation, the randomization of the initial texture was observed due to the grain boundary sliding process (Chokshi et al., 1993). The randomization occurred because each crystal grain rotated independently during the superplastic deformation (Panicker et al., 2009; Xing et al., 2002). However, some exceptions have been reported. For example, Xing et al. induced superplastic deformation on a commercial AZ31 magnesium alloy, which was fine grained initially by multi-directional forging. They confirmed that the crystallographic texture on the basal plane, which was parallel to the tension axis remained even after a superplastic deformation. Furthermore, Watanabe and co-workers examined the texture evolution using a superplastic magnesium alloy (Watanabe et al., 2013). They also confirmed the
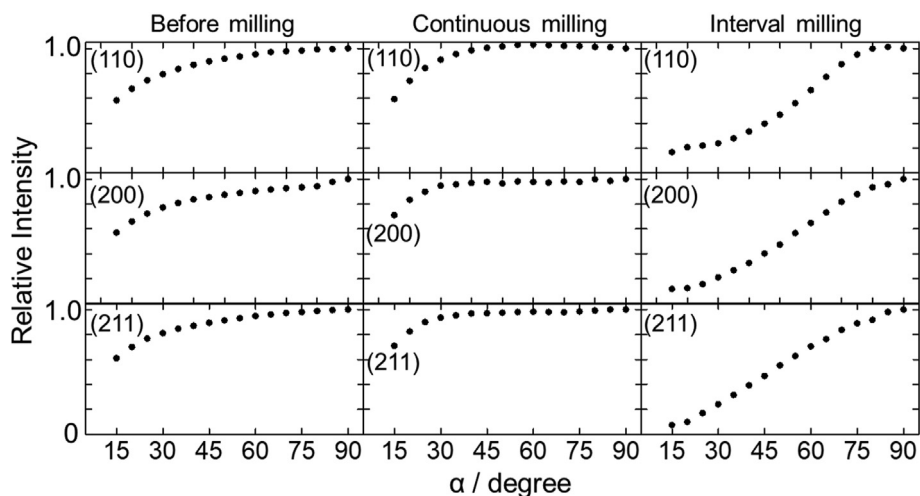
Figure 6. Changes in the relative intensities of the alloy before milling (left), after continuous milling (center) and interval milling (right) with tilt angle (α) using the Schulz reflection method.

convergent evolution of texture that was dependent on the loading direction in the interior of the specimen and the preservation of initial orientation at the near surface of the specimen. They have shown a preservation or evolution of a crystallographic orientation in their specimen that was subjected to a plastic deformation, which was dominated by the grain-boundary-mediated process. In our case, the texture evolution in the alloy particle was likely caused by a stressed condition, which was achieved with the strong friction on the alloy powder surface during the ball-milling process. A discussion on the mechanism involved is beyond the scope of this paper. This work was focused mainly on the effects of friction on an alloy surface to the evolution of crystallographic texture. In the future, we will report a more detailed study on the mechanism using TEM and EBSD analysis.

4. Conclusions

Fe–Si–B–P–Cu nanocrystalline alloy were treated with ball-mill using a lubricant as a process control agent (PCA). Two types of ball-milling methods (i.e., continuous and interval) were conducted to control the interaction between Fe alloy and PCA on the alloy surface. The effect of the interaction on the surface friction and microstructures on the prepared particles were investigated. The alloy sheet was broken into small pieces and deformed plastically into flake-shaped particles, which were obtained using either ball-milling methods. Friction force microscopic analysis of the prepared alloy in the PCA revealed that the friction coefficient on the alloy surface that was exposed to air for a certain period was higher than the alloy surface with a newly generated surface obtained by polishing. From the feature observed from the friction force image, the difference in the friction coefficient was likely induced by the difference in the interaction between the PCA and newly generated surface or surface with oxide due to the exposure to air. During a ball-milling process, the ratio of the newly generated surface to the oxidized surface on the alloy subjected to the interval method was smaller than the alloy subjected to the continuous method. Thus, we considered that the friction coefficient on the surface of the alloy subjected to the interval method was higher. Synchrotron radiation revealed that the alloy subjected to the interval milling enhanced the surface friction and showed an obvious steepness and inflection in the diffraction intensity as a function of the tilt angle in the Schulz reflection method. This indicated a crystallographic texture in the α-Fe grain of the amorphous matrix. Thus, we demonstrated successfully that the ball-milling process induced a crystallographic texture in the Fe-based nanocrystalline alloy by plastic deformation under the condition of enhanced friction

on the surface of the alloy. Finally, the alloy surface was formed by the effect of the interfacial interaction between the alloy and PCA.

Declarations

Author contribution statement

Satoshi Motozuka: Conceived and designed the experiments; Performed the experiments; Analyzed and interpreted the data; Wrote the paper.

Hisashi Sato: Performed the experiments; Analyzed and interpreted the data.

Hidenori Kuwata, Mitsuo Bito: Contributed reagents, materials, analysis tools or data.

Yasuo Okazaki: Conceived and designed the experiments.

Data availability statement

Data included in article/supplementary material/referenced in article.

Declaration of interests statement

The authors declare no conflict of interest.

Additional information

No additional information is available for this paper.

References

Bednarcik, J., Kováč, J., Kollár, P., Roth, S., Sovak, P., Balcerski, J., Polanski, K., Švec, T., 2004. Crystallization of CoFeSiB metallic glass induced by long-time ball-milling. J. Non-Cryst. Solids 337, 42–47.

Boggs, W.E., Kachik, R.H., Pellissier, G.E., 1967. The effects of crystallographic orientation and oxygen pressure on the oxidation of iron. J. Electrochem. Soc. 114 (1), 32.

Buckley, D.H., 1981. Surface Effects in Adhesion, Friction, Wear, and Lubrication, 5. Elsevier, Amsterdam.

Chokshi, A.H., Mukherjee, A.K., Langdon, T.G., 1993. Superplasticity in advanced materials. Mater. Sci. Eng. R Rep. 10, 237–274.

Cui, B.Z., Zheng, L.Y., Waryoba, D., Marinescu, M., Hadjipanayis, G.C., 2011. Anisotropic $SmCo_5$ flakes and nanocrystalline particles by high energy ball-milling. J. Appl. Phys. 109, 07A728.

David, J., 1998. Introduction to Magnetism and Magnetic Materials. CRC Press, Boca Raton, pp. 36–43.

Doig, M., Warrens, C.P., Camp, P.J., 2014. Structure and friction of stearic acid and oleic acid films adsorbed on iron oxide surfaces in squalane. Langmuir 30, 186–195.

Elderton, W.P., Johnson, N.L., 1969. Systems of Frequency Curves. Cambridge University Press, London.

Fujii, H., Tsurekawa, S., Matsuzaki, T., Watanabe, T., 2006. Evolution of a sharp {110} texture in microcrystalline $Fe_{78}Si_9B_{13}$ during magnetic crystallization from the amorphous phase. Phil. Mag. Lett. 86, 113–122.

Gleiter, H., 1991. Nanocrystalline materials. In: Advanced Structural and Functional Materials. Springer, Berlin, Heidelberg, pp. 1–37.

Gulbransen, E.A., Ruka, R., 1952. Role of crystal orientation in the oxidation of iron. J. Electrochem. Soc. 99, 360.

Hasnaoui, A.V., Van Swygenhoven, H., Derlet, P.M., 2002. On non-equilibrium grain boundaries and their effect on thermal and mechanical behaviour: a molecular dynamics computer simulation. Acta Mater. 50, 3927–3939.

He, Y., Shiflet, G.J., Poon, S.J., 1995. Ball-milling-induced nanocrystal formation in aluminum-based metallic glasses. Acta Metall. Mater. 43, 83–91.

Humphreys, F.J., Hatherly, M., 2012. Recrystallization and Related Annealing Phenomena, second ed. Elsevier, Amsterdam.

Iizuka, T., Kita, H., Hirai, T., Osumi, K., 2004. Tribological behavior of W_2C nano-particle reinforced Si_3N_4 matrix composite. Wear 257, 953–961.

Jeon, J.B., Lee, B.J., Chang, Y.W., 2011. Molecular dynamics simulation study of the effect of grain size on the deformation behavior of nanocrystalline body-centered cubic iron. Scripta Mater. 64, 494–497.

Koch, C.C., Whittenberger, J.D., 1996. Mechanical milling/alloying of intermetallics. Intermetallics 4, 339–355.

Kocks, U.F., Tomé, C.N., Wenk, H.R., 1998. Texture and Anisotropy: Preferred Orientations in Polycrystals and Their Effect on Materials Properties. Cambridge University Press, London.

Makino, A., Kubota, T., Yubuta, K., Inoue, A., Urata, H., Matsumoto, H., Yoshida, S., 2011. Low core losses and magnetic properties of $Fe_{85-86}Si_{1-2}B_8P_4Cu_1$ nanocrystalline alloys with high B for power applications. J. Appl. Phys. 109, 7A302-1–7A302-5.

Motozuka, S., Ikeda, T., Miyagawa, T., Sato, H., Morinaga, M., 2017. Formation process of the {001} fiber texture on iron particles using simple ball milling. Powder Technol. 321, 9–12.

Motozuka, S., Tagaya, M., Hayashi, K., Morinaga, M., 2015. Texture formation in iron particles using mechanical milling with graphite as a milling aid. AIP Adv. 5, 097127.

Motozuka, S., Sato, H., Kuwata, H., Bito, M., Okazaki, Y., 2021. Preparation of flake-shaped Fe-based nanocrystalline soft magnetic alloy particles subjected to plastic deformation. Phil. Mag. Lett. 101, 399–407.

Miyake, S., Hashizume, T., Wakatsuki, Y., 2006. Nanoprocessing and evaluation of carbon and boron nitride nanoperiod multilayer films by lateral force modulation method. Surf. Interface Anal. 38, 873–878.

Mizuno, A., Ando, Y., 2010. Scanning probe microscopy for identifying the component materials of a nanostripe structure. Jpn. J. Appl. Phys. 49, 08LB07.

Nieh, T.G., Wadsworth, J., 1991. Hall-Petch relation in nanocrystalline solids. Scripta Metall. Mater. 25, 955–958.

Niu, X., 2020. The study on order behavior and electronic structure of flaky FeSiAl powder. J. Magn. Magn Mater. 493, 165725.

Ovid'ko, I.A., Sheinerman, A.G., 2008. Special rotational deformation in nanocrystalline metals and ceramics. Scripta Mater. 59, 119–122.

Panicker, R., Chokshi, A.H., Mishra, R.K., Verma, R., Krajewski, P.E., 2009. Microstructural evolution and grain boundary sliding in a superplastic magnesium AZ31 alloy. Acta Mater. 57, 3683–3693.

Ramasamy, P., Shahid, R.N., Scudino, S., Eckert, J., Stoica, M., 2017. Influencing the crystallization of $Fe_{80}Nb_{10}B_{10}$ metallic glass by ball-milling. J. Alloys Compd. 725, 227–236.

Schuh, C.A., Nieh, T.G., Yamasaki, T., 2002. Hall–Petch breakdown manifested in abrasive wear resistance of nanocrystalline nickel. Scripta Mater. 46 (10), 735–740.

Schulz, L.G., 1949. A direct method of determining preferred orientation of a flat reflection sample using a Geiger counter X-ray spectrometer. J. Appl. Phys. 20, 1030–1033.

Takaki, S., Masumura, T., Tsuchiyama, T., 2019. Dislocation characterization by the direct-fitting/modified Williamson–Hall (DF/mWH) method in cold worked ferritic steel. ISIJ Int. 59, 567–572.

Takenaka, K., Setyawan, A.D., Sharma, P., Nishiyama, N., Makino, A., 2016. Industrialization of nanocrystalline Fe–Si–B–P–Cu alloys for high magnetic flux density cores. J. Magn. Magn Mater. 401, 479–483.

Tomida, T., 1996. (100)-textured 3% silicon steel sheets by manganese removal and decarburization. J. Appl. Phys. 79, 5443–5445.

Wang, L., Teng, J., Liu, P., Hirata, A., Ma, E., Zhang, Z., Mingwei, C., Han, X., 2014. Grain rotation mediated by grain boundary dislocations in nanocrystalline platinum. Nat. Commun. 5, 1–7.

Watanabe, H., Kurimoto, K., Uesugi, T., Takigawa, Y., Higashi, K., 2013. Accommodation mechanisms for grain boundary sliding as inferred from texture evolution during superplastic deformation. Philos. Mag. A 93, 2913–2931.

Williamson, G.K., Hall, W., 1953. X-ray line broadening from filed Al and W. Acta Metall. 1, 22–31.

Xing, J., Yang, X., Miura, H., Sakai, T., 2002. Continuous dynamic recrystallization in a superplastic 7075 aluminum alloy. Mater. Trans. 43, 2400–2407.